Numerical Methods in Civil Engineering, 7-4 (2023) 35-49

Numerical Methods in Civil Engineering

Journal Homepage: https://nmce.kntu.ac.ir/

Meshless Analysis of a box culvert resting on Modified Vlasov Foundation

FOPA FOUDJI Marius*, TAGOUDJEU Jacques, and LEZIN SEBA MINSILI*****

ARTICLE INFO

RESEARCH PAPER

Article history:
Received:
April 2022.
Revised:
August 2022.
Accepted:
September 2022.

Keywords:
Box culvert,
Winkler foundation,
Modified Vlasov Foundation, RPIM,
Kleinlogel's formulas

Abstract:

In this paper, the computational design of box culverts are compared using Kleinlogel's formulas and three-dimensional models based on Winkler and Modified Vlasov Foundation (MVF) by Radial Point Interpolation method (RPIM). In order to extend the RPIM to the study of box culverts, a method of decomposition is made by subdomain and creation of a fictitious rotation. Similar results are observed between the RPIM_Winkler and STAAD PRO (FEM software), with fewer nodes in the case study. Kleinlogel's formulas or the Winkler model gives a maximal increase in stresses at the middle of the raft of 5% and 12 times increased displacement. Finally, it emerges that for the same type of soil and a single structure, the reaction and shear modulus of the soil is highly depends on the distribution of loads on the structure.

1. Introduction

Box culverts have a variety of useful applications. They are commonly used for bridging purposes, stock and wildlife crossings, drainage structures, and ducting in many industrial applications.

A box culvert is a structure consisting of two parallel slabs monolithically connected to its vertical slabs allowing an opening for waterways and other ways. The simplest plate theory of bending is the classical plate theory (CPT) [1] proposed in the19th century, also called Kirchhoff-Love Theory. In the Classical plate theory, the effects of shear deformation and rotary inertia are ignored. Using this theory in the case of thick plates would result in the overestimation of frequencies [2]. To overcome the drawbacks posed by classical plate theory, Plate Theory [3], Mindlin Plate Theory [4], New First-order a new class of plate theories known as First-order shear deformation theories (FSDT) came into existence (Reissner Shear Deformation Plate [5], …). The primary drawback linked with first-order theories is the difficulty in deciding the correct shear coefficients. The formulation of

first-order theories is such that, they cannot satisfy the shear stress-free surface conditions at the top and bottom surfaces of the plates. To deal with ambiguity in deciding suitable shear coefficients in the case of first-order shear deformation theories, researchers in the field later switched interest to higher-order shear deformation theories (Levinson Plate Theory [6], Reddy Plate Theory [7], Refined Plate Theory [8]). However, Higher-order theories provide a slight increase in accuracy relative to the FSDT solution at the expense of an increase in a computational effort [9].

Generally, the calculation methods used to determine solicitations in the box culvert are based on a two (2D) or a three-dimensional (3D) approach.

The 2D approach is a rescued solution to the 3D problem under simplifying assumptions: the displacements and

* *Corresponding author: Civil Engineer, Department of Civil Engineering, ENSPY, University of Yaounde I, Cameroon, Email: mariusfoudji@yahoo.fr*
** *Lecturer, Department of MSP and Civil Engineering, ENSPY, University of Yaounde I, Cameroon Email: jtagoudjeu@gmail.com*
*** *Assistant Professor, Department of Civil Engineering, ENSPY, University of Yaounde I, Cameroon , Email: lezinsm@yahoo.com*

https://doi.org/10.61186/NMCE.2022.418

forces are assumed to be uniform in the longitudinal direction of the culvert; the analysis is performed considering a unit-wide strip along the longitudinal axe, and this strip issaid to be in plain strain condition. Under these basic assumptions, the plates are assimilated to beams, and the box culvert is analyzed as a two-dimensional frame structure [10-12]. In practice, a model assuming that the bottom slab is infinitely stiff so that it will not undergo any differential settlement is often used. Then, the distribution of the contact pressures on the bottom slab is assumed to be linear, and approximate methods like moment distribution, force or displacement matrix, Kleinlogel's formulas, and FEM are used [10-12] (applications in [13-16]). However, in reality, the bottom slab undergoes differential settlement. Therefore, another model (2D or 3D) considering soil-structure interaction (SSI) is often used to overcome this problem. In this model, the bottom slab is assumed to rest on an elastic foundation, and an SSI model is used to approximate behavior of the foundation soil [11,17]. Some other more sophisticated approaches (2D or 3D) which model the culvert and the soil as a whole system with different constitutive models for soil and structure materials are used in FEM software like ABAQUS, CANDE, and PLAXIS [12].

Several researchers have proposed convenient models to represent the physical behavior of the foundation soil [18-24]. Generally, these models are based on the Winkler approach (local elastic deformation theory) and the Boussinesq model, also known as a continuous elastic model (global elastic deformation theory) [22-23].

The Winkler model is the simplest and most widely used in the theory of bending plates resting on elastic soil. Most of the software have programs that are used today based on this model [22]. According to Winkler, the soil is likened to a series of isolated and independent springs (Winkler 1867) [23]. The stress-strain law is given at priori: the ratio of these two quantities is constant, and it is called the coefficient of stiffness. Therefore, This model excludes the continuity of the deformation from one spring to another through shear forces, which is not very realistic. Besides, the method of determining the coefficient of stiffness of the soil is not unique, which causes problems in choosing this coefficient. Moreover, the works of Vallabhan and Daloglu [25] have shown that this coefficient depends not only on the nature of the soil but also on its depth, the geometry of the structure, the distribution of the loads on the structure, and the rigidity of the foundation. Thus, using of a single coefficient of soil stiffness throughout an entire project is problematic.

To overcome the problems encountered with the Winkler model, researchers have turned to a second model called the "Boussinesq model" or continuous elastic model. Hetenyi [19], Reissner [21], Filonenko-Borodich [18], Pasternak [20], and Kerr [24] have tried to make the Winkler model more realistic by proposing a two-parameter model. Their model considers the effects of shear interactions between different springs, although the shear parameter is determined experimentally. Vlasov and Leont'ev [26] subsequently introduced another arbitrary parameter depending on the characteristics of the base soil of the structure and suggested an approximate value between 1 and 2. The work of Vallabhan and Daloglu [25] subsequently showed how to determine this arbitrary parameter by an iterative procedure in the case of plates, a new method, which they named "modified Vlasov foundation". Here, the continuity of the deformation is also ensured outside the loaded surface. Even though this model is more realistic, it has some mathematical and computational drawbacks, which makes it less applied [23].

In the last decades, several meshless methods have been developed and have made remarkable progress in engineering. In general, meshless methods can be classified into three categories according to the formulation of the equations used [27]. The first class includes methods based on the strong formulation of systems of linear equations, in which the discretization is performed directly from the partial differential equations governing the problem.In this case, the finite difference method [28], the smooth particle hydrodynamic (SPH) method ([29]; [30]), and other collocation methods such as the Kansa collocation method [31] are available. The second class concerns methods based on the weak formulation of systems of equations such as the element-free Galerkin (EFG) method [32], the meshless local Petrov-Galerkin (MLPG) method [33], the Point Interpolation Method (PIM) ([34]; [35]), etc. The third class is related to methods based on the combination of weak and strong formulations such as the meshfree weak-strong-form (MWS) method ([36]; [37]).

Meshless methods have been successfully applied to a wide range of problems, such as free surface [38-41], impact magnetohydrodynamics [42-43], explosion phenomena [44-45], heat conduction [46-47], fracture and crack propagation [48-49], wave propagation [50-51], acoustics and fluid flow [52-53], vibration analysis [54-56], beams [57-58], plates and shells [59-60], and nanoscale mechanics [61-66]. A methodological study on possible and existing meshfree methods is presented in G. R. Liu [67] to solve the partial differential equations governing solid mechanics problems.

The radial point interpolation method (RPIM) is a meshless method based on combining polynomial and radial basis functions [68-70], which has become a widespread technique in the meshfree solution of a wide range of problems. The RPIM has been successfully applied to 1D and 2D solid mechanics [71-73], solution of Kirchoff and Mindlin plates [74-75], analysis of shell problems [76-78], problems of smart materials [79], geometrically non-linear problems [80], material non-linear problems in civil engineering [81], and stress analysis of three-dimensional (3D) solids [82].

In this paper, the comparative study of computational design of box culverts is presented using Kleinlogel's formulas and three-dimensional models based on Winkler and Modified Vlasov Foundation (MVF) using the Radial Point Interpolation method (RPIM). Also,a meshless method for the analysis of box culverts is developed taking into account soil structure interaction using the Winkler model. Comparative results with FEM software (STAAD PRO) are presented to validate the method, in a test case. Also, a Boussinesq approach is used(Modified Vlasov foundation) as a soil-structure interaction model. Next, in a test case, the error made in the analysis of box culverts is numerically evaluated when using a two-dimensional frame structure model assuming a linear distribution of pressure under the bottom slaband Winkler's approach as a soil-structure interaction model, taking Modified Vlasov foundation as the reference model.

This paper is organized as follows: In Section 2, the method of calculation is presented based on the Reissner-Mindlin plate theory. The RPIM approximation method and shear-locking treatment are given in Section 3. In Section 4, we proceed to a comparative analysis between studying a box culvert from the formulas of Adolphe KLEINLOGEL (a two-dimensional model developed for the study of frame box culverts in 1951) and from a three-dimensional model with Winkler's model and modified Vlasov foundation(MVA) model are proceeded. Section 5 is devoted to some concluding remarks and perspectives.

To ease reading, a nomenclature of symbols and parameters used in this paper is presented in Table 1 below.

Table 1: List of symbols and parameters

Symbols	Significations
$\theta_x, \theta_y, \theta_z$	rotations of the mean surface around the axes x, y, and z, respectively
u_I, v_I, w_I	the displacement of node *I* along axes x,y, and z, respectively
α	a parameter
q	a surface density of charge uniformly distributed over the domain Σ
$\bar{q}$	a linear density of charge distributed along the edge $\partial\Sigma_N$;
P_i	concentrated loads at the nodes *i*.
k	a shear correction factor
E	Young's modulus of the material
v	the Poisson's coefficient of the material
h	the thickness of the plate
$\phi_I, \ldots, \phi_n$	the *n* shape functions RPIM
k_0	reaction modulus of foundation soil
k_1	shear modulus of foundation soil
H	depth of the soil
E_F	Young's modulus of the foundation soil.
v_F	the Poisson's coefficient of the foundation soil.
$[K]$	the stiffness matrix of the box culvert
$[S]$	stiffness matrix of the foundation soil
K_e	the stiffness matrix of the plate element
F_e	force vector acting on the plate element
$\{U_e\}$	displacement Vector of nodes of a plate
x_g, y_g, z_g	global axis
x_l, y_l, z_l	local axis
$u^a(x)$	the meshfree approximation of field displacements at a point *x* of a plate
Ka	coefficient of thrust
γ	a dimensionless parameter

2. Method of Calculation

a homogeneous isotropic linear elastic material is considered with the assumption of small deformations.

Here, the Reissner-Mindlin kinematics are used[83] to treat thin and thick plates. The kinematic hypotheses of the Reissner-Mindlin plate theory can be summarized in the following points:

- The material points on a normal to the initial mean surface remain on a straight line in the distorted configuration. This hypothesis makes it possible to take into account the influence of transverse shear deformations;
- The hypothesis of a zero cross-sectional deformation;
- The assumption of plane stresses

For a bending problem of a plate, the field of displacement of a point is defined by:

$$u(x,y,z) = \begin{Bmatrix} z\theta_y(x,y) \\ -z\theta_x(x,y) \\ w(x,y) \end{Bmatrix} \quad (2.1)$$

Where $w(x,y)$ is the transversal displacement of the mean surface of the plate, while; θ_x and θ_y are the rotations of this mean surface around the two axes x and y, respectively. *2.1 Problem of the sixth degree of freedom*

In Reissner's theory, which used for the study of plates, the rotation around the normal is not supplied with rigidity, and therefore, there are only five (05) effective degrees of freedom. The difficulty is associated with rotation around the

normal and it is called the "sixth degree of freedom problem". To overcome this problem, the technique proposed by Bui Hung Cuong is used [84], which introduces a fictitious shear deformation given by:

$$\gamma_{xy}^{*} = \alpha\theta_z \qquad (2.2)$$

Where θ_z is the rotation of the mean surface around the z-axis at a given point, and α is a parameter.

α *is taken* 0 to eliminate the influence of this fictitious rigidity.

2.2 Elementary matrices

Here, a principle similar to the finite element method will be used, thus each of the four plates forming the box culvert is considered as an element. For each element, Figure 1 illustrates a surface density of charge q uniformly distributed over the domain Σ a linear density of charge $\bar{q}$ distributed along the edge $\partial\Sigma_N$ and concentrated loads P_i at the nodes *i*.

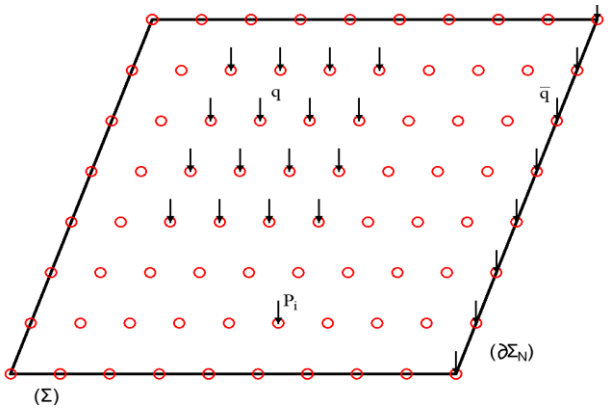

Fig. 1: Graphical illustration of a plate

In the local coordinate system to the element, the stiffness matrix of the plate, K_e, and the force vector, F_e, are given by the equations.

$$K_e = \int_{\Sigma} [B_b^T C_b B_b + B_m^T C_m B_m + B_s^T C_s B_s] d\Sigma \qquad (2.3)$$

$$F_e = \int_{\Sigma} N_w^T q d\Sigma + 6 \int_{\partial\Sigma_N} N_w^T \bar{q}\, d\partial\Sigma_N + \sum_i N_{wi} P_i \qquad (2.4)$$

where

$B_b, B_m, and\ B_s$ are matrices related to bending moments, normal forces, and shear forces, respectively;

q : a surface density of charge uniformly distributed over the domain Σ ;

$\bar{q}$: a linear density of charge distributed along the edge $\partial\Sigma_N$;

P_i : concentrated loads at the nodes *i*.

The matrices in equations (2.3) and (2.4) are given by Equations (2.5) - (2.11), thus:

$$C_b = \frac{Eh^3}{12(1-v^2)} \begin{bmatrix} 1 & v & 0 \\ v & 1 & 0 \\ 0 & 0 & \frac{(1-v)}{2} \end{bmatrix} \qquad (2.5)$$

$$C_m = \frac{Eh}{12(1-v^2)} \begin{bmatrix} 1 & v & 0 \\ v & 1 & 0 \\ 0 & 0 & \frac{(1-v)}{2} \end{bmatrix} \qquad (2.6)$$

$$C_s = \frac{kEh}{2(1+v)} \begin{bmatrix} 1 & 0 & 0 \\ 0 & 1 & 0 \\ 0 & 0 & 1 \end{bmatrix} \qquad (2.7)$$

Where k is a shear correction factor with a value of 5/6, E and v are Young's modulus of the material, and Poisson's coefficient, respectively, while h is the thickness of the plate.

$$B_b = \begin{bmatrix} 0 & 0 & 0 & 0 & \phi_{I,x} & 0 & \cdots & \cdots & 0 & 0 & 0 & 0 & \phi_{n,x} & 0 \\ 0 & 0 & 0 & -\phi_{I,y} & 0 & 0 & \cdots & \cdots & 0 & 0 & 0 & -\phi_{n,y} & 0 & 0 \\ 0 & 0 & 0 & -\phi_{I,x} & \phi_{I,y} & 0 & \cdots & \cdots & 0 & 0 & 0 & -\phi_{n,x} & \phi_{n,y} & 0 \end{bmatrix} \qquad (2.8)$$

$$B_s = \begin{bmatrix} 0 & 0 & 0 & 0 & 0 & \alpha & \cdots & \cdots & 0 & 0 & 0 & 0 & 0 & \alpha \\ 0 & 0 & \phi_{I,x} & 0 & \phi_I & 0 & \cdots & \cdots & 0 & 0 & \phi_{n,x} & 0 & \phi_n & 0 \\ 0 & 0 & \phi_{I,y} & -\phi_I & 0 & 0 & \cdots & \cdots & 0 & 0 & \phi_{n,y} & -\phi_{n,x} & 0 & 0 \end{bmatrix} \qquad (2.9)$$

$$B_m = \begin{bmatrix} \phi_{I,x} & 0 & 0 & 0 & 0 & 0 & \cdots & \cdots & 0 & 0 & 0 & 0 & \phi_{n,x} & 0 \\ 0 & \phi_{I,y} & 0 & 0 & 0 & 0 & \cdots & \cdots & 0 & 0 & 0 & -\phi_{n,y} & 0 & 0 \\ \phi_{I,y} & \phi_{I,x} & 0 & 0 & 0 & 0 & \cdots & \cdots & 0 & 0 & 0 & -\phi_{n,x} & \phi_{n,y} & 0 \end{bmatrix} \qquad (2.10)$$

$$N_w = [0 \quad 0 \quad \phi_I \quad 0 \quad 0 \quad 0 \quad \cdots \quad \cdots \quad 0 \quad 0 \quad \phi_n \quad 0 \quad 0 \quad 0] \qquad (2.11)$$

Where $\phi_I, \ldots, \phi_n$ are the *n*-shape functions RPIM (Section 3), with *n* being the number of nodes distributed on the plate. The internal forces in the element are approximated by the equations:

$$M(u) \cong C_b B_b U \qquad (2.12)$$

$$Q(u) \cong C_s B_s U \qquad (2.13)$$

$$N(u) \cong C_m B_m U \qquad (2.14)$$

M, N, Q representing the vectors of bending moments, normal forces, and shear forces, respectively, while U is the displacement vector of the nodes of the element such that

$$U^T = [u_I \quad v_I \quad w_I \quad \theta_{xI} \quad \theta_{yI} \quad \theta_{zI} \quad \cdots \quad \cdots \quad u_n \quad v_n \quad w_n \quad \theta_{xn} \quad \theta_{yn} \quad \theta_{zn}] \qquad (2.15)$$

2.3 Soil foundation modeling

2.3.1 Winkler model

Winkler (1867) assumed that the vertical translation of the soil *w* at a point depends only on the contact pressure *p* acting at that point in the idealized elastic foundation and a proportionality constant *k*. Afterwards, the relationship between the external pressure and the deflection of the foundation surface under pressure is expressed as [85-86]:

$$p = kw \quad (2.16)$$

The proportionality constant, *k*, is called "the modulus of subgrade reaction" of the soil.
According to the Winkler model, the expression of the strain energy, U_F , in the foundation is given by the following relation [85-86]:

$$U_F = \frac{k}{2}\iint w^2 dxdy \quad (2.17)$$

Discretizing the integral in (2.17), it is:

$$U_F = \frac{k}{2}\{U\}^T \iint [N_w]^T[N_w]dxdy\,\{U\} \quad (2.18)$$

Also written:

$$U_F = \tfrac{1}{2}\{U\}^T[S]\{U\} \quad (2.19)$$

With:

$$[S] = k\iint [N_w]^T[N_w]dxdy \quad (2.20)$$

The rigidity matrix of the foundation soil corresponds to the plate element, while *k* is the reaction modulus of the foundation soil.

2.3.2 Modified Vlasov Model (MVF)

In the two-parameter model of Vlasov for a plate resting on an elastic foundation, including a shear effect of the foundation, the expression relating the pressure and the corresponding defection of the foundation is [85-86]:

$$p = k_0 w - k_1\left(\frac{\partial^2 w}{\partial x^2} + \frac{\partial^2 w}{\partial y^2}\right) \quad (2.21)$$

Where $p, w, and\ k_1$ are the surface pressure, the transverse defection, and the shear modulus of the foundation (second foundation parameter), respectively, while k_0 is the modulus of subgrade reaction of the soil (first or Winkler foundation parameter).
According to the Vlasov model, the expression of the strain energy, U_F , in the foundation is given by the following relation [85-86]:

$$U_F = \frac{k_0}{2}\iint w^2 dxdy + \frac{k_1}{2}\iint (\nabla w)^2 dxdy \quad (2.22)$$

Discretizing the integral in (2.22), we have:

$$U_F = \frac{k_0}{2}\{U\}^T \iint [N_w]^T[N_w]dxdy\,\{U\} +$$

$$\frac{k_1}{2}\{U\}^T \iint \left[\frac{\partial N_w}{\partial x}, \frac{\partial N_w}{\partial y}\right]^T \left[\frac{\partial N_w}{\partial x}, \frac{\partial N_w}{\partial y}\right] dxdy\,\{U\} \quad (2.23)$$

Also written as:

$$U_F = \tfrac{1}{2}\{U\}^T[S]\{U\} \quad (2.24)$$

With:

$$[S] = k_0\iint [N_w]^T[N_w]dxdy + k_1\iint \left[\frac{\partial N_w}{\partial x}, \frac{\partial N_w}{\partial y}\right]^T \left[\frac{\partial N_w}{\partial x}, \frac{\partial N_w}{\partial y}\right] dxdy \quad (2.25)$$

The rigidity matrix of the foundation soil corresponds to the plate element, while k_0 and k_1 are reaction and foundation soil shear modulus, respectively.

Assuming the modulus of elasticity of the soil E_F is constant in a finite depth *H* of the soil, the soil moduli k_0 and k_1 in (2.25) are given by the relations [44, 51]:

$$k_0 = \frac{E_F(1-v_F)}{8H(1+v_F)(1-2v_F)}\frac{2\gamma sinh2\gamma + 4\gamma^2}{sinh^2\gamma} \quad (2.26)$$

$$k_1 = \frac{E_F H}{16\gamma^2(1+v_F)}\frac{2\gamma sinh2\gamma - 2\gamma^2}{sinh^2\gamma} \quad (2.27)$$

Where v_F is the Poisson coefficient of the foundation soil. However, these parameters also depend on a coefficient representing the rate at which the foundation soil declines and displacements, and normal stresses in the vertical direction. According to Vallabhan, Straughan and Das [86], this parameter can be expressed as:

$$\left(\frac{\gamma}{H}\right)^2 = \frac{(1-2v_F)}{2(1-v_F)}\frac{\int_{-\infty}^{+\infty}\int_{-\infty}^{+\infty}(\nabla w)^2 dxdy}{\int_{-\infty}^{+\infty}\int_{-\infty}^{+\infty} w^2 dxdy} \quad (2.28)$$

For plates resting on elastic soil, the dimensionless parameter can be evaluated using an iterative procedure after determining vertical displacement, as shown by Vallabhan and al. [86].

2.4 Modeling plate-soil system (sill plate)

To analyze the phenomenon of soil-structure interaction, the deformation energy in the foundation will be added to that of the plate. The total potential energy of the plate-soil system is then written:

$$\Pi = \frac{1}{2}\{U\}^T[K]\{U\} + \frac{1}{2}\{U\}^T[S]\{U\} - \{F\}\{U\}^T \quad (2.29)$$

By applying the principle of minimizing potential energy, as follows:

$$\frac{\partial \Pi}{\partial\{U\}} = [K]\{U\} + [S]\{U\} - \{F\} = 0 \quad (2.30)$$

Which gives the following global system:

$$\left[K_g\right]\{U\} = \{F\} \text{ with } \left[K_g\right] = [K] + [S] \quad (2.31)$$

Where $[K_g]$ is the rigidity matrix of the plate resting on an elastic foundation

2.5 Geometric transformation matrix

Considering the stiffness matrices being defined in the local coordinate system associated with the plate, all the quantities of each plate must be brought to a common axis system of the structure. the global axis y_g is always choosen parallel to the local axis y_l (Figure 2), and the geometric transformation should only be executed in the *xz*-plane.

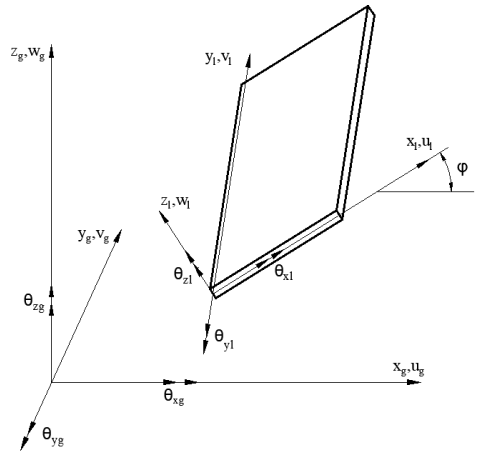

Fig. 2: Global and local axis systems

In matrix form, for a node *i* [84]

$$\{U\}_{ig} = [T]\{U\}_{il} \qquad (2.32)$$

with

$$[T] = \begin{bmatrix} cos\varphi & 0 & -sin\varphi & 0 & 0 & 0 \\ 0 & 1 & 0 & 0 & 0 & 0 \\ sin\varphi & 0 & cos\varphi & 0 & 0 & 0 \\ 0 & 0 & 0 & cos\varphi & 0 & -sin\varphi \\ 0 & 0 & 0 & 0 & 1 & 0 \\ 0 & 0 & 0 & sin\varphi & 0 & cos\varphi \end{bmatrix} \qquad (2.33)$$

Thus, for a plate comprising *n* nodes, the transformation matrix of size (6n * 6n) becomes:

$$[R] = \begin{bmatrix} T & 0 & \dots & 0 \\ 0 & \ddots & 0 & \vdots \\ \vdots & 0 & \ddots & 0 \\ 0 & \dots & 0 & T \end{bmatrix} \qquad (2.34)$$

hence,

$$\{U\}_g = [R]\{U\}_l \qquad (2.35)$$

Now, the loading has to be linked to the displacements in the reference, given the relation in the reference linked to the plate as $\{F_e\}_l = [K_e]_l\{U_e\}_l$. The relationship between the two force vectors in the axis systems, as follows:

$$\{F_e\}_g = [R]\{F_e\}_l \quad (2.36)$$

Afterwards:

$$\{F_e\}_g = [R][K_e]_l\,[R]^T\{U_e\}_g = [K_e]_g\{U_e\}_g \quad (2.37)$$

The relation between the expressions of the stiffness matrix in the two references is thus obtained from the following: $[K_e]_g = [R][K_e]_l\,[R]^T$

2.6 Numerical integration

In order to make this method truly without meshes, asa method of numerical integration, the Cartesian transformation method is used (CTM) [87].

3. The RPIM shape functions

The meshfree approximation of field displacements at a point *x* of a plate is denoted by $u^a(x)$, and given by the following expression [86,88]:

$$u^a(x) = [p^T(x)A + r^T(x)B]u(x) \qquad (3.1)$$

or

$$u^a = \begin{bmatrix} u^a \\ v^a \\ w^a \\ \theta_x^a \\ \theta_y^a \\ \theta_z^a \end{bmatrix} = \sum_{I=1}^{n} \begin{bmatrix} \phi_I(x) & 0 & 0 & 0 & 0 & 0 \\ 0 & \phi_I(x) & 0 & 0 & 0 & 0 \\ 0 & 0 & \phi_I(x) & 0 & 0 & 0 \\ 0 & 0 & 0 & \phi_I(x) & 0 & 0 \\ 0 & 0 & 0 & 0 & \phi_I(x) & 0 \\ 0 & 0 & 0 & 0 & 0 & \phi_I(x) \end{bmatrix} \begin{bmatrix} u_I \\ v_I \\ w_I \\ \theta_{xI} \\ \theta_{yI} \\ \theta_{zI} \end{bmatrix} \qquad (3.2)$$

Without prejudice to generality, in the rest of the sequel, the symbol "*a*" will be omitted in Equation (3.2). Hence, as follows:

$$u = \begin{bmatrix} u \\ v \\ w \\ \theta_x \\ \theta_y \\ \theta_z \end{bmatrix} = \sum_{I=1}^{n} \Phi_I \mathrm{U}_I \qquad (3.3)$$

with

$$\Phi_I = \begin{bmatrix} \phi_I(x) & 0 & 0 & 0 & 0 & 0 \\ 0 & \phi_I(x) & 0 & 0 & 0 & 0 \\ 0 & 0 & \phi_I(x) & 0 & 0 & 0 \\ 0 & 0 & 0 & \phi_I(x) & 0 & 0 \\ 0 & 0 & 0 & 0 & \phi_I(x) & 0 \\ 0 & 0 & 0 & 0 & 0 & \phi_I(x) \end{bmatrix}$$

Where $\mathrm{U}_I = \left(u_I, v_I, w_I, \theta_{xI}, \theta_{yI}, \theta_{zI}\right)^T$ is the displacement vector at node *I* while ϕ_I is the shape function defined by:

$$\phi_I(x) = \sum_{j}^{m} p_j(x)A_{jI} + \sum_{k}^{n} r_k(x)B_{kI} \qquad (3.4)$$

In this work, to limit shear-locking effects, increase the degree of the interpolation polynomial will be in creased [89-90].

The matrices **A** and **B** are defined by [88,91]:

$$A = (P^T R^{-1} P)^{-1} P^T R^{-1} \quad (3.5)$$

$$B = R^{-1}(I - PA) \quad (3.6)$$

Where I is an identity matrix, and $p(x)$ in Equation (3.1) is a polynomial with m basic functions

$$p^T(x) = [p_1(x), p_2(x), \dots, p_m(x)] \quad (3.7)$$

For n nodes distributed over the domain, the matrix P of size n x m is expressed as:

$$P = \begin{bmatrix} p_1(x_1) & p_2(x_1) & \cdots & p_m(x_1) \\ p_1(x_2) & p_2(x_2) & \cdots & p_m(x_2) \\ \vdots & \vdots & \ddots & \vdots \\ p_1(x_n) & p_2(x_n) & \cdots & p_m(x_n) \end{bmatrix} \quad (3.8)$$

The term $r(x)$ in Equation (3.1) is given by:

$$r^T(x) = [R(x_1, x), R(x_2, x), \dots, R(x_n, x)] \quad (3.9)$$

Where $R(x_i, x_j)$ is a basic radial function and

$$R = \begin{bmatrix} R(x_1, x_1) & R(x_1, x_2) & \cdots & R(x_1, x_n) \\ R(x_2, x_1) & R(x_2, x_2) & \cdots & R(x_2, x_n) \\ \vdots & \vdots & \ddots & \vdots \\ R(x_n, x_1) & R(x_n, x_2) & \cdots & R(x_n, x_n) \end{bmatrix} \quad (3.10$$

In this work, as follows:

- Radial basis function, the polynomial spline defined by $R(x_i, x_j) = r_{ij}^5$ where $r_{ij} = \|x_i - x_j\|$ is the Euclidean distance between the two points.

- polynomial $p^T(x) = [1 \quad x \quad y \quad x^2 \quad xy \quad y^2 \quad x^2y \quad xy^2]$

The first derivatives of the shape function can be obtained as:

$$\phi_{I,i}(x) = \sum_j^m p_{j,i}(x) A_{jI} + \sum_k^n r_{k,i}(x) B_{kI} \quad (3.11)$$

The shape functions thus defined have the Kronecker delta property:

$$\phi_I(x_j) = \delta_{Ij} = \begin{cases} 1 \; si \; I = j \\ 0 \; si \; I \neq j \end{cases} \quad (3.12)$$

4. Case study of a Box culvert

In what follows, the results will be presented obtained by:

- STAAD Pro software (MEF software using the Winkler model);
- The formulas of KLEINLOGEL ;
- RPIM using Winkler foundation (RPIM_Winkler) ;
- RPIM using modified Vlasov foundation (RPIM_Vlasov).

The results presented here are obtained using, for each of the four (04) plates a mesh of 40x40 for the STAAD Pro software and nodes distributed according to a mesh of 10x10 in the RPIM, which has 15 times lesser nodes in RPIM than in STAAD Pro.

4.1 General presentation of the box culvert

It is a box culvert of 1.80 x1.80 m2 section on which rests a 10 cm thick asphalt concrete pavement. The apron, raft, and piers are all 20 cm thick and made of reinforced concrete (Figure 3)

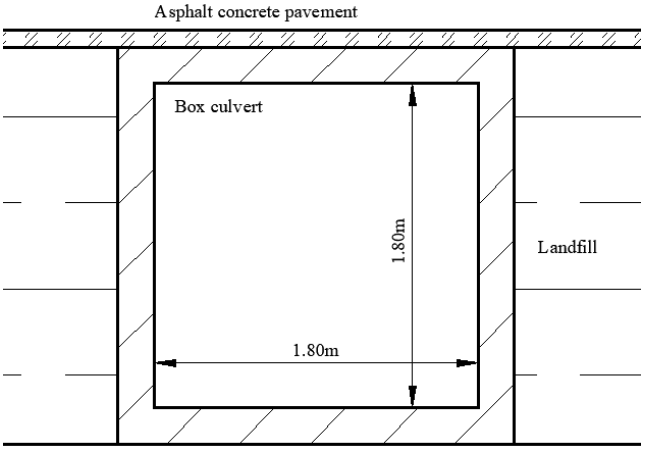

Fig. 3: Presentation of the box culvert

The 2D modeling is obtained by the mean surface (Figure 4):

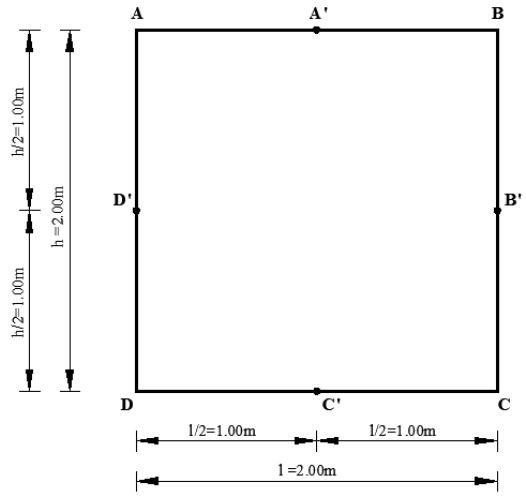

Fig. 4: Modeling at the mean surface

4.2 Materials characteristics

The characteristics of materials are given in **Table 2** below.

Table 2: Materials characteristic of the study case [92]

Materials	Characteristic
Concrete	Density 2.5t/m3

Landfill	Density 1.8t/m3
	Coefficient of thrust $Ka = 0.27$
	Overburden on the landfill 1.5 t/m2
Soil foundation	Young's modulus $E_F = 10MPa$
	Poisson ratio $v_F = 0.25$
	Depth of soil $H = 2m$
	Soil reaction modulus: $k = 3000KN/m^3$ (using the semi-empirical Vlasov model [93])

4.3 Actions

The structure is submitted to four (04) actions:

- The weight of the road and the self-weight (G1);
- The thrust of land (G2);
- The action of the traffic (Q1): a concentrated load $P = 6t$ is considered at the center of the deck,
- The action of the overburden on the landfill (Q2).

The analysis will be done on a one-meter length.

02 Combinations of loads is used:

- Ultimate Limited States (ULS): 1.35*(G1+G2) + 1.5*(Q1+Q2)
- Service Limited States (SLS): G1 + G2 + Q1 + Q2

4.4 Presentation of results

4.4.1 Deformation of the structure and foundation soil

The combined effect of these loads on the structure at SLS gives a maximum displacement at the middle of the deck of 17.9 mm with the model of Winkler and 1.5 mm with a modified Vlasov foundation. Figure 4 and 5 show the final deformation of the box culvert when all the loads are applied at the same time on the structure. In fact, there are the displacements of each point of the structure .

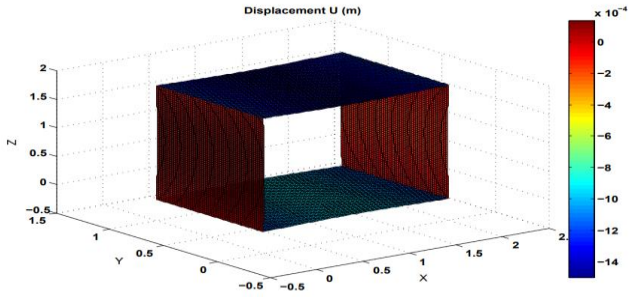

Fig. 5: Deformation of the structure – Modified Vlasov model (Scale 100:1)

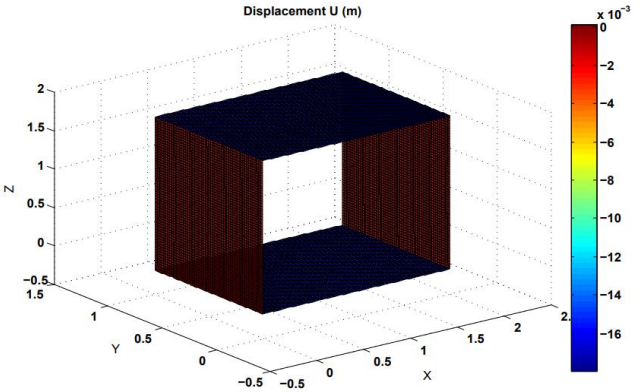

Fig. 6: Deformation of the structure – Winkler model (Scale 10:1)

Figures 7 and 8 show the soil deformation, using the Vlasov and Winkler models, respectively. For a better visibility, different scales have been chosen for these representations

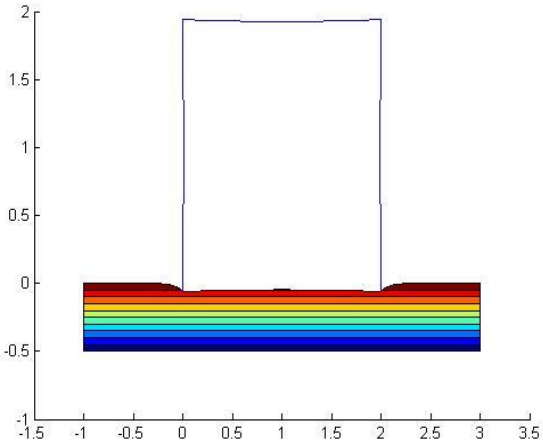

Fig. 7: Deformation of soil foundation – Modified Vlasov model (Scale 50:1)

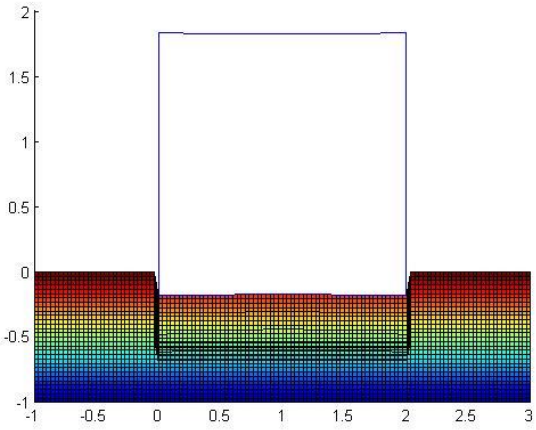

Fig. 8: Deformation of soil foundation–Winkler model (Scale 10:1)

It is observed that:

- The maximum displacement obtained by the Winkler model is 12 times greater than that obtained by the Modified Vlasov Model.
- There is a continuity of deformations around the loaded surface in the Modified Vlasov Model, which is more realistic than the deformations in the Winkler model.

In the following, the results obtained by the Modified Vlasov model are considered as a basic result for error estimation.

4.4.2 Bending moments and displacements

The bending moments along the local x-axis (*Mxx*) and the displacement along the local z-axis of some characteristic points of the structure are presented, when the box culvert is subjected to the different loads taken separately.

4.4.2.1 Weight of the roadway and self-weight

The results of the bending moments along the x-axis obtained are presented in Table 3:

Table 3: Bending moments along the *x*-axis due to the weight of the roadway and self-weight

Weight of the roadway and self-weight (KN/m)							
PTS	RPIM Vlasov	KLEINLOGEL		RPIM_Winkler		STAAD PRO	
	Value	Value	Error (%)	Value	Error (%)	Value	Error (%)
A	-0.900	-0.830	7.778	-0.875	2.778	-0.88	2.222
D	-3.238	-3.300	1.915	-3.369	4.046	-3.34	3.15
A'	2.908	3.000	3.164	2.910	0.069	2.931	0.791
C'	5.196	5.400	3.926	5.413	4.176	5.451	4.908
D'	-2.044	-2.065	1.027	-2.097	2.593	-2.112	3.327

The displacements at the centers of the deck, raft, and piers are given in Table 4.

Table 4: Displacement at element's centers due to the weight of the roadway and self-weight

Weight of the roadway and self-weight (mm)					
PTS	RPIM Vlasov	RPIM_Winkler		STAAD PRO	
	Value	Value	W/V	Value	W/V
A'	-0.5816	-7.6000	13.07	-7.6200	13.10
C'	-0.4319	-7.5000	17.37	-7.4700	17.30
D'	-0.0486	-0.0498	1.02	-0.0470	0.97

W/V: ratio of Winkler displacement by Vlasov displacement

These Vlasov results are obtained from the three (03) parameters presented in Table 5:

Table 5: Vlasov parameters: the case of the weight of roadway and self-weight

γ	$k_0(KN/m^3)$	$k_1(KN/m)$
16.1161	48 348.300	248.200

γ, k_0, k_1 being calculated from equations (2.28), (2.26), and (2.27), respectively

4.4.2.2 Thrust of land

The results of the bending moments along the x-axis obtained are presented in Table 6:

Table 6: Bending moments along the x-axis due to the thrust of land

The thrust of land (KN/m)							
PTS	RPIM Vlasov	KLEINLOGEL		RPIM_Winkler		STAAD PRO	
	Value	Value	Error (%)	Value	Error (%)	Value	Error (%)
A	-0.742	-0.730	1.617	-0.748	0.809	-0.745	0.404
D	-0.937	-0.890	5.016	-0.904	3.522	-0.889	5.123
A'	-0.733	-0.730	0.409	-0.740	0.955	-0.739	0.819
C'	-0.828	-0.890	7.488	-0.889	7.367	-0.888	7.246
D'	1.623	1.620	0.185	1.635	0.739	1.643	1.232

The displacements at the centers of the deck, raft, and piers are given in table 7.

Table 7: Displacement at element's centers due to the thrust of land

The thrust of land (mm)					
POINTS	RPIM Vlasov	RPIM_Winkler		STAAD PRO	
	Value	Value	W/V	Value	W/V
A'	0.0306	0.0313	1.02	0.0300	0.98
C'	-0.0071	-0.0075	1.06	-0.0070	0.99
D'	0.0305	0.0308	1.01	0.0300	0.98

W/V: ratio of Winkler displacement by Vlasov displacement

These Vlasov results are obtained from the three (03) parameters presented in Table 8.

Table 8: Vlasov parameters: the case of the thrust of land

γ	$k_0(KN/m^3)$	$k_1(KN/m)$
18.9596	56 878.800	210.970

γ, k_0, k_1 being calculated from equations (2.28), (2.26), and (2.27), respectively

4.4.2.3 Overburden on the landfill

The results of the bending moments along the x-axis obtained are presented in Table 9:

Table 9: Bending moments along the x-axis due to the overburden on the landfill

Overburden on the landfill (KN/m)							
PTS	RPIM Vlasov	KLEINLOGEL		RPIM_Winkler		STAAD PRO	
	Value	Value	Error (%)	Value	Error (%)	Value	Error (%)
A	-0.682	-0.675	1.026	-0.687	0.733	-0.683	0.147
D	-0.714	-0.675	5.462	-0.689	3.501	-0.681	4.622
A'	-0.675	-0.675	0.000	-0.680	0.741	-0.679	0.593
C'	-0.631	-0.675	6.973	-0.678	7.448	-0.677	7.290
D'	1.353	1.350	0.222	1.363	0.739	1.360	0.517

The displacements at the centers of the deck, raft, and piers are given in Table 10.

Table 10: Displacement at element's centers due to the weight of the overburden on the landfill

Overburden on the landfill (mm)					
PTS	RPIM Vlasov	RPIM_Winkler		STAAD PRO	
	Value	Value	W/V	Value	W/V
A'	0.0261	0.0266	1.02	0.0260	1.00
C'	-0.0054	-0.0057	1.06	-0.0050	0.93
D'	0.0255	0.0257	1.01	0.0250	0.98

W/V: ratio of Winkler displacement by Vlasov displacement

These Vlasov results are obtained from the three (03) parameters presented in Table 11:

Table 11: Vlasov parameters: the case of the overburden on the landfill

γ	$k_0(KN/m^3)$	$k_1(KN/m)$
18.9563	56 868.900	211.010

γ, k_0, k_1 being calculated from equations (2.28), (2.26), and (2.27), respectively.

4.4.2.4 Traffic

The results of the bending moments along the x-axis obtained are presented in Table 12:

Table 12: Bending moments along the x-axis due to the traffic

Traffic (KN/m)							
PTS	RPIM Vlasov	KLEINLO-GEL		RPIM_Win-kler		STAAD PRO	
	Value	Value	Error (%)	Value	Error (%)	Value	Error (%)
A	-8.202	-8.120	1.000	-8.151	0.622	-8.200	0.024
D	-4.248	-4.375	2.990	-4.511	6.191	-4.500	5.932
A'	21.037	21.880	4.007	21.088	0.242	20.600	2.077
C'	10.011	10.620	6.083	10.632	6.203	10.600	5.884
D'	-6.092	-6.250	2.594	-6.197	1.724	-6.200	1.773

The displacements at the centers of deck, raft and piers are given in Table 13.

Table 13: Displacement at element's centers due to the weight of the traffic

Traffic (mm)					
PTS	RPIM Vlasov	RPIM_Winkler		STAAD PRO	
	Value	Value	W/V	Value	W/V
A'	-1.0000	-10.4000	10.40	-10.4100	10.41
C'	-0.5501	-9.9000	18.00	-9.9300	18.05
D'	-0.1450	-0.1473	1.02	-0.1330	0.92

W/V: ratio of Winkler displacement by Vlasov displacement

These Vlasov results are obtained from the three (03) parameters presented in Table 14:

Table 14: Vlasov parameters: the case of the traffic

γ	$k_0(KN/m^3)$	$k_1(KN/m)$
16.2313	48 693.900	246.440

γ, k_0, k_1 being calculated from equations (2.28), (2.26), and (2.27), respectively.

4.5 Interpretation of results

Following these results obtained in this work, various observations are made on the two Vlasov parameters, bending moments, and displacements.

4.5.1 Two parameters of Vlasov

Figures 9 and 10 show that for the same foundation soil and the same rigidity of the structure, the reaction and soil shear moduli are strongly influenced by the distribution of loads on the structure. This result is is consistent with the result presented in the work of Vallabhan and Daloglu (1999) [25], showing that the soil reaction modulus depends not only on the nature of the soil but also on its depth, the geometry of the structure, the distribution loads on the structure and the rigidity of the foundation (Vallabhan and Daloglu, 1999) [25].

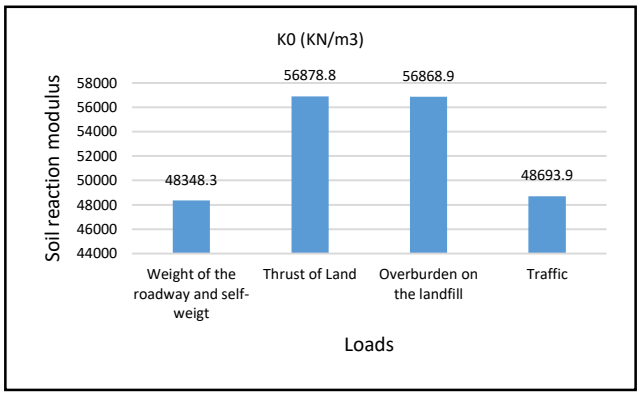

Fig. 9: Variation of soil reaction modulus with the distribution of loads

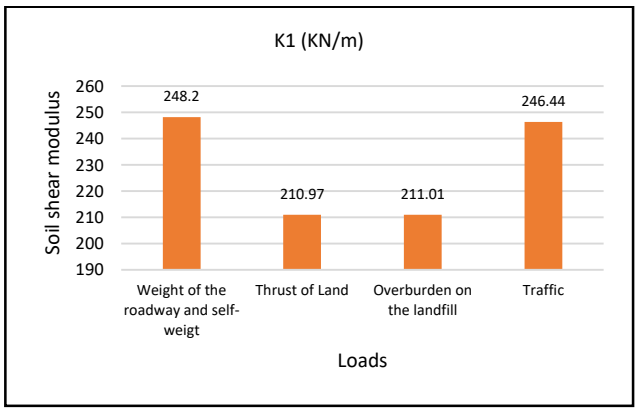

Fig. 10: Variation of soil shear modulus with the distribution of loads

These results show that using a single soil reaction modulus in the Winkler model for the entire project is problematic.

4.5.2 Bending moments

The influence of the soil model on the distributions of bending moments on the box culvert at ULS is presented in Table 15.

Table 15: Bending moments along x at ULS

ULS (KN/m)							
PTS	RPIM Vlasov	KLEINLOGEL		RPIM_Winkler		STAAD PRO	
	Value	Value	Error (%)	Value	Error (%)	Valeur	Error (%)
A	-15.455	-15.299	1.009	-15.357	0.634	-15.518	0.408
D	-12.908	-13.232	2.510	-13.412	3.905	-13.481	4.39
A'	33.430	34.872	4.313	33.528	0.293	32.841	1.762
C'	20.079	21.006	4.617	21.104	5.105	21.045	4.811
D'	-7.680	-7.951	3.529	-7.882	2.630	-7.893	2.773

Table 15 shows that the Winkler model or KLEINLOGEL's formulas increase bending moments up to 5% on the box culvert, which induces a general overestimation of bending reinforcements in the structure. The maximum increase in bending moments is observed at the center of the raft.

4.5.3 Displacements

When the loads are applied perpendicular to the structure (traffic, self-weight, superstructure), the displacements at the center of the raft and deck are 10 to 18 times larger in the Winkler model than those in the Modified Vlasov model. Also, the displacements at the center of the piers are similar in both methods. Besides, when the loads are applied horizontally to the structure (thrust of land, overburden on the landfill), the displacements obtained by the two models are quite close. If in the service limited states (SLS), the combined effect of these loads on the structure is considered, the maximum displacement on the box culvert is observed to be 12 times greater when the Winkler model foundation is used, as opposed to the modified Vlasov foundation.

Consequently:

- The tridimensional meshless method developed for the analysis of box culverts allows to have satisfactory results;
- Winkler foundation modeling generally makes it possible to oversize the structure;
- Modified Vlasov foundation provides better results than Winkler's because it is more realistic than the latter one, taking into consideration the continuity of displacement around the box culvert.
- Soil reaction and shear moduli can't be taken as a constant when analyzing the behavior of a structure.

5. Conclusion

In this paper, the study of the behavior of box culverts by the RPIM is discussed and a comparative study between the use of the formulas of Adolphe KLEINLOGEL (which assume that box culvert is a two-dimensional frame structure with a linear distribution of soil pressure at the bottom of the slab) and the use of a three-dimensional model of box culvert are made taking into accounts soil structure interaction (SSI) using Winkler model or Modified Vlasov model of soil foundation behavior. In order to extend RPIM applied to the plates in the study of box culverts, a method of decomposition by subdomain and creation of a fictitious rotation was made. Considering simulations made on a box culvert , the STAAD PRO software (FEM software), and the program developed on MATLAB, it is observed that:

- The meshless approach developed shows similar results (bending moments and displacements) with those obtained with STAAD PRO under the same assumptions, with fewer nodes in the case study.
- There is a continuity of deformations around the loaded surface in the Modified Vlasov Model, which is more realistic than the deformations in the Winkler model.
- Instead of using a Boussinesq model as an SSI model, considering a box culvert as a two-dimensional frame structure without accounting for SSI (or as a three-dimensional structure resting on a Winkler foundation), an increase in bending moments up to 5% on the box culvert, and a 12 times increase in the displacement on the box culvert are observed.
- For the same soil type and structure, the reaction modulus and the soil shear modulus are highly dependent on the distribution of loads on the structure. These moduli can't be taken as constants for a type of soil and foundation, as generally done by engineers using software based on the Winkler model.

Despite these results obtained, the use of a global meshless method in this work induces much calculation time and space memory. To improve this work, we propose using a local meshless method. Further perspectives can be the applications of the assumed mode method (AMM), which has proved his efficiency for the mechanical analysis of embedded plates ([94,95] and the references therein) for the analysis of box culverts.

References

[1] Y. M. Ghugal and R P Shimpi (2002), A review of refined shear deformation theories of isotropic and anisotropic laminated plates, *J. Reinf. Plast. Compos.*, Vol. 21, pp. 775-813

[2] R.A. Shetty, Dushyanthkumar G.L., Deepak S.A. (2018), Classical and Refined Beam and Plate Theories: A Brief Technical Review, *Sahyadri International Journal of Research*; 4(2), pp27-32

[3] E. Reissner (1945), The effect of transverse shear deformation on the bending of elastic plates, *J. Appl. Mech.*, Vol. 12, pp69-77

[4] R. D. Mindlin (1951), Influence of rotary inertia and shear on flexural motions of isotropic, elastic plates, *J. Appl. Mech.*, Vol. 18, pp. 31-38,

[5] R. P. Shimpi, H. G. Patel and H. Arya (2007), New first-order shear deformation plate theories, *J. Appl. Mech.*, Vol. 74, pp. 523-533

[6] M. Levinson (1980), An accurate, simple theory of the statics and dynamics of elastic plates, *Mech. Res. Commun.* Vol. 7, pp. 343-350

[7] J. N. Reddy (1984), A simple higher-order theory for laminated composite plates, *J. Appl. Mech.*, Vol. 51, pp. 745-752

[8] R. P. Shimpi (2002), Refined plate theory and its variants, *AIAA J*, Vol. 40, pp. 137-146

[9] C.M. Wang, J.N. Reddy, K.H. Lee (2000), Shear Deformable Beams and Plates: Relationships with classical solutions, ISBN 978-0-08-043784-2

[10] Ajay R.P., S.P. Chandresha, K.B. Parikh (2017), A review paper on analysis and cost-comparison of box culvert for different aspect ratio of cell, *International Journal of Engineering Trends and Technology*, 44 (3), pp112-115

[11] M.G. Kalyanshetti, S.V. Malkhare (2012), Analysis of box considering soil structure interaction, *Indian Journal of Research*, 1(4), pp71-74

[12] W.D. Lawson, H. Seo, J.G. Surles, S.M. Morse (2017), Culvert Rating Guide, Second Edition, Texas Department of Transportation, pp1-196

[13] Oladejo J.S., Adetoye O.A. (2022), Reliability evaluation of reinforced concrete box culvert at Qua Plateau State Nigeria, *International Journal of Research Publication and reviews*, 3(6), pp2884-2893

[14] T. Deshmukh, V. Kadlag (2022), Analysis of box culvert under cushion loading, *International Journal of Innovative Research in science Engineering and Technology (IJIRSET)*, 11(6), pp7735-7742

[15] Prema S.B., Guruprasad T.N., T.V. Mallesh, S.R. Ramesh (2019), Parametric study on behaviour of RCC box culvert for dynamic loading, *International Research Journal of Engineering and Technology (IRJET)*, 6(9), pp96-103

[16] A.D. Patil, A.A. Galatage (2016), Analysis of box culvert under cushion loading, *International Advanced Research Journal in Science Engineering and Technology (IARJSET)*, 3(6), pp163-166

[17] Saurav, I. Pandey (2017), Economic design of RCC Box culvert through comparative study of conventional and finite element method, *International Journal of Engineering and Technology (IJET)*, 9(3), pp1707-1713

[18] Filonenko-Borodich MM (1940), Some approximate theories of elastic foundation, *Uchenyie Zapiski Moskovskogo Gosudarstvennogo Universitet, Mekhanika*, 46, 3-18. (in Russian)

[19] Hetenyi M. (1950), A general solution for the bending of beams on an elastic foundation of arbitrary continuity, *Journal of Applied Physics*, 21(1), 55-58

[20] Pasternak PL. (1954), New method of calculation for flexible substructures on two-parameter elastic foundation, *Gosudarstvennoe Izdatelstoo. Literatury po Stroitelstvu i Architekture*, Moskau, 1-56. (in Russian).

[21] Reissner E. (1958), A note on deflections of plates on a viscoelastic foundation, *Journal of Applied Mechanics ASME*, 25(1):144-145

[22] Mohamed El-Hebib GUELLIL (2012), Modeling of the behaviour of plates resting on elastic soil by the finite element method, *Master thesis, Hassiba Ben Bouali University of Chlef*, pp.1-175.

[23] Rabinovivi, A. (1970), Reciprocal action between the structure and the foundation soil, *Technical bulletin of French-speaking Switzerland*, 9, pp. 131-137

[24] Kerr A.D. (1964), Elastic and Viscoelastic foundation models, *Journal of Applied Mechanics*, 31, pp491- 498

[25] Vallabhan CVG, Daloglu AT. (1999), Consistent FEM-Vlasov model for plates on layered soil, *Journal of Structural Engineering ASCE*, 125(1), pp108-113

[26] Vlasov VZ, Leont'ev NN (1960), Beams, plates and shells on elastic foundations. *GIFML, Moskau*. (in Russian)

[27] G.R. Liu, Y.T. Gu (2005), An Introduction to Meshfree Methods and Their Programming Springer, Dordrecht, The Netherlands

[28] T. Liszka, J. Orkisz (1980), The finite difference methods at arbitrary irregular grids and its applications in applied mechanics, *Computers & Structures*, 11, pp. 83-95

[29] L. Lucy (1977), A numerical approach to testing the fission hypothesis, *The Astronomical Journal*, 82, pp. 1013-1024

[30] G.R. Liu, M.B. Liu (2003), Smoothed Particle Hydrodynamics - A Meshfree Practical Method, *World Scientific, Singapore, 472page*

[31] R.L. Hardy (1990), Theory and applications of the multiquadrics-biharmonic method (20 years of discovery 1968–1988), *Computers & Mathematics with Applications*, 19, pp. 163- 208

[32] T. Belytschko, Y.Y. Lu, L. Gu (1994), Element-free Galerkin methods, *International Journal for Numerical Methods in Engineering*, 37, pp. 229-256

[33] S.N. Atluri, T. Zhu (1998), A new meshless local Petrov-Galerkin (MLPG) approach in computational mechanics, *Computational Mechanics*, 22, pp. 117-127

[34] G.R. Liu, Y.T. Gu (2001), A point interpolation method for two-dimensional solids, *International Journal for Numerical Methods in Engineering*, 50, pp. 937-951

[35] G.R. Liu (2002), Meshfree Methods: Moving Beyond the Finite Element Method, CRC Press, Boca Raton, USA

[36] G.R. Liu, Y.T. Gu (2003), A meshfree method: meshfree weak–strong (MWS) form method, for 2-D solids, *Computational Mechanics*, 33 (1), pp. 2-14

[37] G.R. Liu, Y.L. Wu, H. Ding (2004), Meshfree weak–strong (MWS) from method and its application to incompressible flow problems, *International Journal for Numerical Methods in Fluids*, 46, pp. 1025-1047

[38] L. Cueto-Felgueroso, I. Colominas, F. Navarrina, M. Casteleiro (2005), Numerical simulation of free surface flows by Lagrangian particle methods, *Journal of Fluid Structure Interaction and Moving Bounadary Problems*, 84, pp. 1-9

[39] G. Shobeyri, M.H. Afshar (2010), Simulating free surface problems using Discrete Least Squares Meshless method, *Computers and Fluids Journal*, pp461-470

[40] F. Daneshmand, M. Kazemzadeh-Parsi (2004), A Meshless Method for Free Surface Flow Through Sluice Gates, *6th International Conference on Hydroinformatics*, pp71-78

[41] W.C. Moon, H.T. Puay, T.L. Lau (2018), Numerical simulation of free surface flow using a multiphase model with higher order scheme, *Conference in Advances in civil engineering and science technology*, pp 1-8

[42] V.C. Loukopoulos, G.C. Bourantas, E.D. Skouras (2011), Localized meshless point collocation method for time-dependent magnetohydrodynamics flow through pipes under a variety of wall conductivity conditions, *Computational Mechanics Journal*, 47, pp137-159

[43] Philip F.H., Matthias J.R. (2016), Accurate meshless methods for magnetohydrodynamics, *Monthly Notices of the Royal Astronomical Society*; 455(1), pp51-88

[44] B.K. Ferezgdhi, R. Naderi (2017), A Numerical Modeling for Underwater Explosion Using Mesh-Less Smooth Particle Hydrodynamics Method, *Advanced Defence Sci. and Tech.*, 7; pp161-169

[45] D. Hu, L. Chunhan, X. YiHua, X. Han (2014), Analysis of explosion in concrete by axisymmetric FE-SPH adaptive coupling method; *Engineering Computations*, 31(4), pp 758-774

[46] M. Afrasiabi, M. Roethlin, K. Wegener (2019), Contemporary Meshfree Methods for Three Dimensional Heat Conduction Problems, *Archives of Computational Methods in Engineering*, 27; pp1413-1447

[47] R.J. Cheng, K.M. Liew (2012), A meshless analysis of three-dimensional transient heat conduction problems, *Engineering Analysis with Boundary Elements*, 36(2), pp203-210

[48] M.T. Mohammadi Anaei, A. Khosravifard, T.Q. Bui (2021), Analysis of fracture mechanics and fatigue crack growth in moderately thick plates using an efficient meshfree approach, *Theoretical and Applied Fracture Mechanics*, 113; 102943

[49] N. Fallah, N. Nikraftar (2018), Meshless finite volume method for the analysis of fracture problems in orthotropic media, *Engineering Fracture Mechanics*, 204, pp46-62

[50] S.M. Hosseini, C. Zhang (2021), Band structure analysis of Green-Naghdi-based thermoelastic wave propagation in cylindrical phononic crystals with energy dissipation using a meshless collocation method, *International Journal of Mechanical Sciences*, 209; 106711

[51] J. Ma, H. Gao, G. Wei, J. Qiao (2020), The meshless analysis of wave propagation based on the Hermit-type RRKPM, *Soil Dynamics and Earthquake Engineering*, 134, 106154

[52] M.N. Rasoulizadeh, M.J. Ebadi, Z. Avazzadeh, O. Nikan (2021), An efficient local meshless method for the equal width equation in fluid mechanics, *Engineering Analysis with Boundary Elements*, 131; pp258-268

[53] S. Shahriari, D. Garcia (2018), Meshfree simulations of ultrasound vector flow imaging using smoothed particle hydrodynamics, *Physics in Medicine and Biology*, 63(20), pp1-18

[54] J.F. Wang, J.P. Yang, S.K. Lai, W.Zhang (2020), Stochastic meshless method for nonlinear vibration analysis of composite plate reinforced with carbon fibers, *Aerospace Science and Technology*, 105, 105919

[55] N. Fallah, M. Delzendeh (2018), Free vibration analysis of laminated composite plates using meshless finite volume method, *Engineering Analysis with Boundary Elements*, pp132-144

[56] S. Hosseini, G. Rahimi, Y. Anani (2021), A meshless collocation method based on radial basis functions for free and forced vibration analysis of functionally graded plates using FSDT, *Engineering Analysis with Boundary Elements*, 125, pp168-177

[57] J. Li, Y. Guan, G. Wang, G. Zhao, J. Lin, H. Naceur, D. Coutellier (2018), Meshless modeling of bending behaviour of bi-directional functionally graded beam structures, *Composites Part B: Engineering*, 115; pp 104-111

[58] G. Giunta, S. Belouettar, A.J.M. Ferreira (2016), A static analysis of three-dimensional functionally graded beams by hierarchical modelling and a collocation meshless solution method, *Acta Mechanica*, 227, pp969-991

[59] H. Mellouli, H. Jrad, M. Wali, F. Dammak (2019), Meshless implementation of arbitrary 3D-shell structures based on a modified first order shear deformation theory, *Computers and Mathematics with Applications*, 77(1): pp34-39

[60] K.M. Liew, X. Zhao, A.J.M. Ferreira (2011), A review of meshless methods for laminated and functionally graded plates and shells, *Composite Structures*, 93(8): pp2031-2041

[61] P. Jankowski, K.K. Zur, A. Farajpour (2022), Analytical and meshless DQM approaches to free vibration analysis of symmetric FGM porous nanobeams with piezoelectric effect, *Engineering Analysis with Boundary Elements*, 136, pp266-289

[62] K. Kiani (2022), Nonlocal-integro-surface energy-vibro analysis of twist in coaxially composite wire-like nanostructures with internal and interfacial defects via a meshless technique, *Engineering Analysis with Boundary Elements*, 135, pp217-232

[63] X. Wang, H. Qi, Z. Sun, L. Hu (2019), A van der Waals contact-bond model for low-dimensional nanoscale carbon materials based on the quasi-continuum method, *Journal of Materials Research*, 34(24): pp 4011-4023

[64] S. Saitta, R. Luciano, R. Vescovini, N. Fantuzzi, F. Fabbrocino (2022), Optimization of a Radial Point Interpolation Meshless strategy for strain gradient nanoplates, *Engineering Analysis with Boundary Elements*, 140, pp70-78

[65] M. Rezaiee-Pajand, M. Mokhtari (2019), A novel meshless particle method for nonlocal analysis of two-directional functionally graded nanobeams, *Journal of the Brazilian Society of Mechanical Sciences and Engineering*, 41, 303

[66] R. Ansari, A. Arjangpay (2014), Nanoscale vibration and buckling of single-walled carbon nanotubes using the meshless local Petrov–Galerkin method, *Physica E: Low-dimensional Systems and nanostructures*, 63, pp283-292

[67] G. R. Liu (2016), An Overview on Meshfree Methods: For Computational Solid Mechanics, *Int J of Computational Methods*, 13(5):1-42

[68] Liu, G. R., Zhang G. Y., Gu Y. T. and Wang Y. Y. (2005), A meshfree radial point interpolation method (RPIM) for three-dimensional solids, *Comput Mech*, 36, pp421–430.

[69] Wang, J. G. and Liu, G. R. (2002a), A point interpolation meshless method based on radial basis functions, *Int. J. Numer. Meth. Engng*, 54, pp1623–1648.

[70] Wang, J. G. and Liu, G. R. (2002b), On the optimal shape parameters of radial basis functions used for 2D meshless methods, *Comput. Methods Appl. Mech. Engrg*., vol. 191, pp. 2611-2630.

[71] Gu YT, Liu GR (2001), A local point interpolation method for static and dynamic analysis of thin beams, *Comput Methods Appl Mech Eng*, 190, pp5515–5528

[72] Liu GR, Gu YT (2001b), A local radial point interpolation method(LR-PIM) for free vibration analyses of 2-D solids. *J Sound Vib*, 246(1), pp29–46

[73] Liu GR, Yan L, Wang JG, Gu YT (2002), Point interpolation method based on local residual formulation using radial basis functions, *Struct Eng Mech*, 14(6), pp713–732

[74] Dinis, L.M.J.S., Natal Jorgea, R.M. and Belinha, J. (2008), Analysis of plates and laminates using the natural neighbour radial point interpolation method, *Engineering Analysis with Boundary Elements*, 32, 267 –279.

[75] Liu, Y., Hon Y. C. and Liew K. M. (2006), A meshfree Hermite-type radial point interpolation method for Kirchhoff plate problems, *Int. J. Numer. Meth. Engng*, 66: 1153–1178.

[76] Liu, L., Chua L.P. and Ghista D.N. (2006), Conforming radial point interpolation method for spatial shell structures on the stress-resultant shell theory, *Arch Appl Mech*, 75, 248–267.

[77] Zhao, X., Liu, G. R., Dai K. Y., Zhong Z. H., Li G. Y. and Han X. (2009a), Free-vibration analysis of shells via a linearly conforming radial point interpolation method (LC-RPIM), *Finite Elements in Analysis and Design*, 45, pp917–924.

[78] Zhao, X., Liu, G. R., Dai K. Y., Zhong Z. H., Li G. Y. and Han X. (2009b), A linearly conforming radial point interpolation method (LC-RPIM) for shells, *Comput Mech*, 43, pp403–413

[79] Liu L, Liu GR, Tan VBC (2002) Element free method for static and free vibration analysis of spatial thin shell structures. *Comput Methods Appl Mech Eng* 191(51–52):5923–5942

[80] Omar A, Said M, Bouazza B (2020) On the use of Radial Point Interpolation Method (RPIM) in a high order continuation for the resolution of the geometrically nonlinear elasticity problems. *Engineering Analysis with Boundary Elements*, vol 110, pp 69-79

[81] Wang JG, Liu GR, Lin P (2002) Numerical analysis of Biot's consolidation process by radial point interpolation method. *Int J Solids Struct*, 39(6), pp1557–1573

[82] G. R. Liu, G. Y. Zhang, Y. T. Gu, Y. Y. Wang (2005) A meshfree radial point interpolation method (RPIM) for three-dimensional solids. *Comput Mech*, 36, pp421-430

[83] Code Aster (2016), Plate elements: modeling DKT, DST, DKTG and Q4g, Version 12, pp.1-58

[84] Bui Hung Cuong (2008), Static analysis of the behaviour of thin-walled structures by the finite element method and finite strips of the plate type and lowered shell deformable in shear, *PhD Thesis, University of Lierge*, pp.1-209

[85] R. Buczkowski, W. Torbacki (2009), Finite element analysis of plate on layered tensionless foundation, *Archives of Civil Engineering*, LVI, 3, pp. 255-274

[86] Vallabhan CVG, Straughan W.T, Das YC. (1991), Refined model for analysis of plates on elastic foundations, *Journal of Engineering Mechanics ASCE*, 117(12):2830-2844

[87] A. Khosravifard and M. R. Hematiyan (2010), A new method for meshless integration in 2D and 3D Galerkin meshfree methods, *Engineering Analysis with Boundary Elements*, 34, pp. 30-40

[88] T. Q. Bui and Ch. Zhang (2011), A moving Kriging interpolation-based element-free Galerkin method for structural dynamic analysis, *Computer Methods in Applied Mechanics and Engineering*, 200, 1354-1366.

[89] O. Garcia, E. A. Fancello, C. S. de Barcellos et C. A. Duarte (2000), hp-Clouds in Mindlin's thick plate model, *International Journal for Numerical Methods in Engineering*, 47(8),1381–1400

[90] P. de T. R. Mendonc¸a, C. S. de Barcellos, et A. Duarte (2000), In vestigetions on the hp-cloud method by solving timoshenko beam problems, *Computational Mechanics*, 25(2–3):286–295

[91] T.Q. Bui and al. (2016), High frequency modes meshfree analysis of Reissner-Mindlin plates, *Advanced Materials and Devices*, 1, pp. 400-412

[92] MESSI Alfred (2011), Dimensioning of an ordinary rectangular box culvert, Project, pp. 1-47

[93] S. Imanzadeh, A. Marache, A. Denis (2011), Estimation of the variability of the reaction modulus for the study of the behaviour of strip footings on elastic soil: Application from existing models, *XXIXe Civil Engineering University Meetings*, Tlemcen, pp. 1-10

[94] D. Cho, B.H. Kim, J. Kim, N. Vladimir, T. Choi (2017), Simplified dynamic analysis of stepped thickness rectangular plate structures by the assumed mode method, *Part M: Journal of Engineering for the Maritime Environment*, 231(1), pp. 177-187

[95] Kiani, K., Gharebaghi, S.A. and Mehri, B. (2017), In-plane and out-of-plane waves in nanoplates immersed in bidirectional magnetic fields, *Structural engineering and mechanics: An international journal*, 61(1), pp.65-76.